Phase diagram of mixed monolayers of stearic acid and dimyristoylphosphatidylcholine. Effect of the acid ionization

Franco Vega Mercado, Bruno Maggio, Natalia Wilke *

Centro de Investigaciones en Química Biológica de Córdoba (CIQUIBIC), Dpto. de Química Biológica, Facultad de Ciencias Químicas, Universidad Nacional de Córdoba, Pabellón Argentina, Ciudad Universitaria, X5000HUA Córdoba, Argentina

ARTICLE INFO

ABSTRACT

The aim of this work is to study the phase diagram of mixed monolayers composed of dimyristoylphosphatidylcholine (DMPC) and stearic acid (SA) at different ionic strength and bulk pH of the aqueous subphase. In this way, the effect of ionization of SA on the interaction and thus on phase separation with the DMPC matrix can be analyzed. To this purpose, we first determined the ionization state of pure SA monolayers as a function of the bulk subphase pH. The SA monolayers are nearly fully ionized at pH 10 and essentially neutral at pH 4 and the mixture of DMPC and SA was studied at those two pHs. We found that the DMPC-enriched phase admits more SA if the SA monolayer is in a liquid-expanded state, which is highly related to the acid ionization state, and thus to the bulk pH and ionic strength. At pH 4 the molecules hardly mix while at pH 10 the mixed monolayer with DMPC can admit between 30 and 100% of SA (depending on the lateral pressure) before phase separation is established. The addition of calcium ions to the subphase has a condensing effect on SA monolayers at all pHs and the solubility of SA in the DMPC matrix does not depend on the bulk pH in these conditions. The observed phase diagrams are independent on the manner in which the state of the mixed film is reached and may thus be considered states of apparent equilibrium.

© 2011 Elsevier Ireland Ltd. All rights reserved.

1. Introduction

Cellular membranes contain a significant fraction of anionic surfactants; electrostatics is thus expected to contribute to the energetics and stability of biomembranes. Of the numerous biological functions that take place at the membrane level, many are influenced (or even dominated) by electrostatic interactions (Langner and Kubica, 1999; Mengistu et al., 2010; Hermelink and Brezesinski, 2008). The charge on a surfactant (and thus its mixing properties) can be controlled by varying the environment properties: ionic strength, pH and membrane composition. On the other hand, it is well recognized that the complex interplay of interactions within a lipid membrane leads, in general, to nonideal mixing properties (Almeida, 2009) which enables it to laterally organize the structure with formation of segregated domains, and locally adjust the lipid composition (Villasuso et al., 2010). Furthermore, it has been shown that the presence of phase segregation can be a regulating factor in the activity of phospholipases (Fanani et al., 2002, 2010) thus accentuating the role of non-random lipid mixing on activity.

Monolayers at the air–water interface are extremely valuable model membranes (Brockman, 1999; McConnell, 1991; Möhwald et al., 1995; Möhwald, 1990; Vollhardt, 2002). Experiments in which molecular area, surface pressure, temperature and chemical nature of the subphase are varied can easily be performed and, by this means, a broad set of thermodynamic parameters, which characterize the monolayer can be accurately determined (Gaines, 1966; Adamson, 1982). Although transmembrane processes cannot be studied in monolayers, this system is well suited for studying lateral mixing and structuring mediated by a variety of lipids and proteins of biomembranes (Maggio, 1994; Brezesinski and Möhwald, 2002; Maggio et al., 2006, 2008; Fanani et al., 2010).

Mixed monolayers composed of phospholipids with fatty acids have been studied previously under different conditions and exploring different effects (Maggio and Lucy, 1975, 1976; Bringezu et al., 2001; Koynova and Tenchov, 2001; Roach et al., 2004; Romão and Gonçalves da Silva, 2004; Schmidt et al., 2001; Schullery et al., 1981; Templer et al., 1998). However, to our knowledge no systematic study of the phase diagram or of the detailed effect of ionization on miscibility and domain topography was carried out in this kind of mixtures. The aim of this work is to study the mixing properties of monolayers composed of dimyristoylphosphatidylcholine (DMPC) and stearic acid (SA) at different ionic strength and bulk pHs. The detailed phase diagram was explored, with an emphasis on the influence of charge in the miscibility of the SA molecules in

* Corresponding author. Tel.: +54 351 433 4171; fax: +54 351 433 4171.
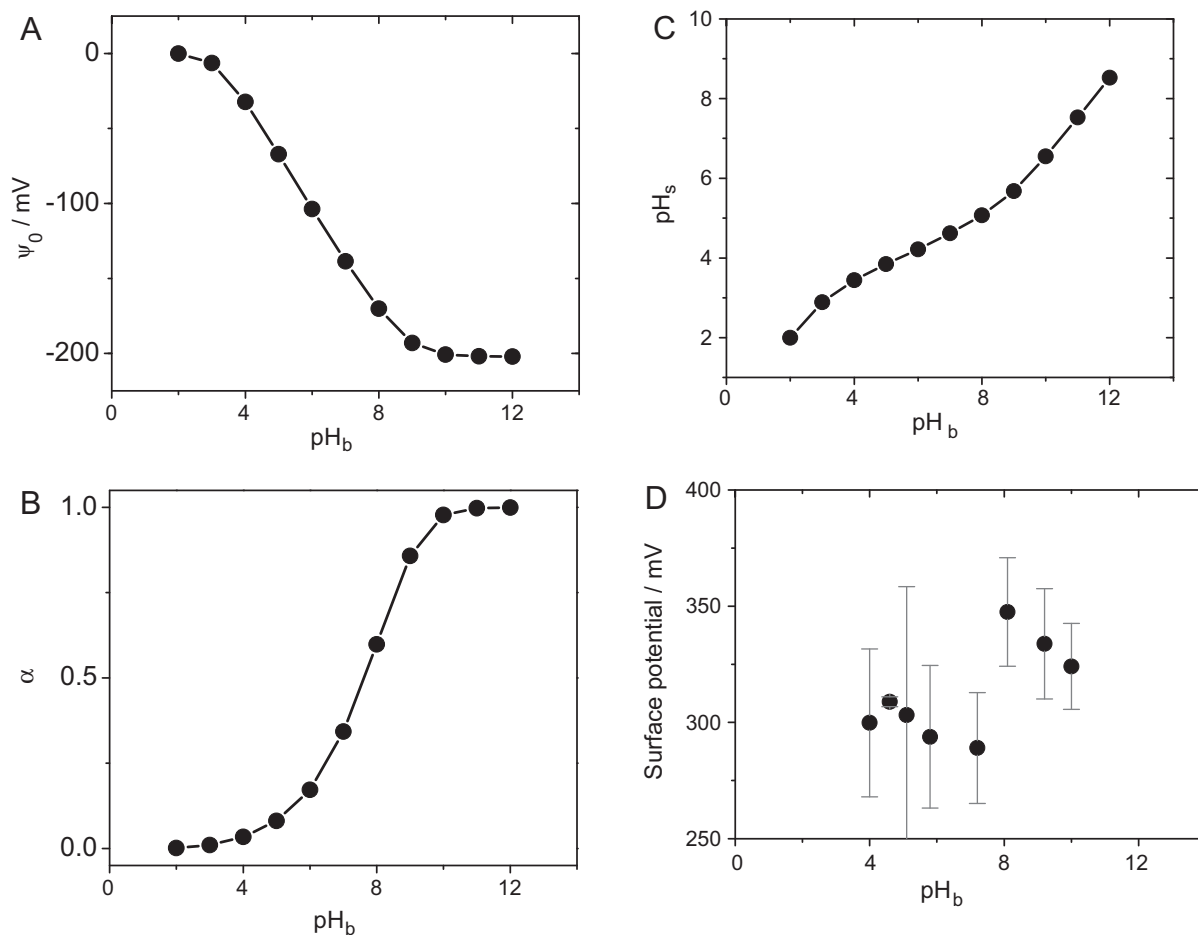*E-mail address:* wilke@mail.fcq.unc.edu.ar (N. Wilke).

Fig. 1. Theoretical and experimental surface parameters as a function of the bulk pH for monolayers of stearic acid at 0.25 nm^2 and 20 °C on subphases with EDTA 10 mM and TRIS 10 mM. (A) Double layer potential at the surface, (B) degree of ionization of the stearic acid, (C) surface pH and (D) dipole potential (surface potential after subtracting the double layer potential taken from (A)). The error bars correspond to the standard deviation of at least three independent measurements.

order to provide an understanding on molecular terms of the effect of ionization of SA on the interaction with DMPC.

The ionization state of pure SA monolayers was first determined at each bulk pH (Section 3.1). We found that the SA monolayers are fully ionized at pH 10 and neutral at pH 4. At these pHs, the phase diagram of the mixture was explored using the compression isotherms and "in situ" monolayer images (Sections 3.2 and 3.3). The effect of Ca^{2+} ions was also studied. Finally, we compared the phase state of the monolayer reached by compression with that reached by changes of pH, corroborating that the phase diagrams obtained represent a state of apparent equilibrium (Section 3.4).

2. Material and methods

2.1. Materials

Stearic acid (SA), dimyristoylphosphatidylcholine (DMPC) and the lipophilic fluorescent probe L-α-phosphatidylethanolamine-N-(lissamine rhodamine B sulfonyl) ammonium salt (Chicken Egg-Transphosphatidylated) were purchased from Avanti Polar Lipids (Alabaster, AL, USA). Solvents and chemicals were of the highest commercial purity available. The water used for the subphase was from a MilliQ system (Millipore) with a resistivity of 18 MΩ cm and a surface tension of 72 mN m^{-1}. The surfactant monolayers were prepared and characterized in different Langmuir film balances under isometric compression (KSV minithrough, KSV Instruments, Ltd., and microthrough, Kibron, Helsinki, Finland), at 20 ± 1 °C on subphases of 10 mM

tris(hydroxymethyl)aminomethane (TRIS) and 10 mM Ethylenedi-aminetetraacetic acid (EDTA) with or without NaCl 0.5 M at pH 4 and 10. The pH was adjusted with the acid and base species of the TRIS and EDTA buffers. EDTA was added in order to chelate the biva-lent ion impurities possible present in the solutions since very low concentration of these ions can modify the monolayer properties of SA (Deamer et al., 1967).

The ion concentration in both subphase solutions is high enough to screen electrostatic interactions (the ionic strength and the Debye length are 25 mM and 0.2 nm for the solution without NaCl and 250 mM and 0.05 nm for the solutions with NaCl). However, to the purpose of simplification we will call "low" ionic strength solution the solution without NaCl salt.

2.2. Compression isotherms

Lateral pressure and surface potential were simultaneously reg-istered while the monolayer was isometrically compressed at about 10^{-2} nm^2 s^{-1} molecule^{-1}. The lateral pressure was determined with a Pt plate using the Wilhelmy method and the surface poten-tial was measured with an air-ionizing ^{241}Am surface electrode and a Ag/AgCl/Cl$^-$ (3 M) reference electrode (Wilke and Maggio, 2009).

2.3. Phase diagrams

Each zone in the phase diagram at each pH was determined from the lateral pressure-mean molecular area compression isotherms and from the observation of the monolayer using Brewster angle
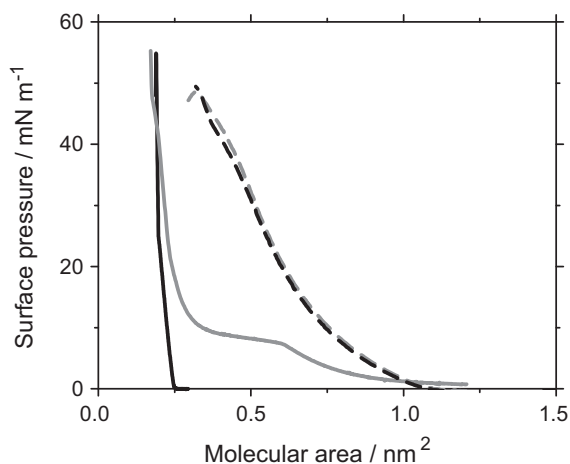
Fig. 2. Surface pressure-average molecular area compression isotherms for dimyristoylphosphatidylcholine (dashed lines) and for stearic acid (solid lines) at 20 °C on subphases that contain NaCl 0.5 M, EDTA 10 mM and TRIS 10 mM at pH 4 (black lines) and 10 (grey lines).

Fig. 3. Representative micrographs for monolayers of dimyristoylphosphatidylcholine and stearic acid in the indicated lipid proportions and surface pressures obtained with Brewster angle microscopy at 20 °C. Subphase composition: NaCl 0.5 M, EDTA 10 mM and TRIS 10 mM, pH 4. Images size: 150 μm × 185 μm.

microscopy (BAM) or fluorescence microscopy (FM) while simultaneously registering the lateral pressure and mean molecular area of the monolayer. For the BAM experiments we used an EP3 Imaging ellipsometer (Accurion, Goettingen, Germany) with a 20× or a 10× objective and the monolayer was spread in a Langmuir film balance (KSV minithrough, KSV Instruments, Ltd., Helsinki, Finland). For the FM experiments, the fluorescent probe was incorporated in the lipid solution before spreading (1 mol%). The Langmuir film balance (microthrough, Kibron, Helsinki, Finland) was placed on the stage of an inverted fluorescence microscope (Axiovert 200, Carl Zeiss, Oberkochen, Germany) with a 20× objective. Images were registered by a EMCCD video camera (IXON).

2.4. Monolayer thickness calculation

Each phase thickness (h) was calculated from the BAM images taken after the BAM equipment was calibrated. The grey level of each section of the micrograph can then be converted to reflected light intensity (R_p), and h was calculated assuming a smooth but thin interface in which the refractive index varies along the normal of the interface on a distance h, much smaller than the incident light wavelength λ (Lhevender et al., 2000), which leads to:

$$h = \frac{\sqrt{R_p}}{\sin(2\theta_B - 90)} \left(\frac{\pi \sqrt{n_1^2 + n_2^2}(n_1^2 - n^2)(n_2^2 - n^2)}{\lambda(n_1^2 - n_2^2)n^2} \right)^{-1} \quad (1)$$

In Eq. (1), n_1 and n_2 are the film, air and subphase refractive index, respectively and θ_B is the Brewster angle.

The refractive indexes used were 1.44 for the SA monolayer and for the condensed phase (Petrov et al., 1999), 1.43 for the DMPC monolayers and the expanded phase (Ducharme et al., 1999) and 1.00 for the air; for the subphase the refractive index was calculated for each experiment from the experimental Brewster angle. The values obtained were 1.34 for the subphases with NaCl 0.5 M and 1.33 for the subphases without NaCl.

3. Results and discussion

3.1. Ionization state of SA as a function of the bulk pH

The acid constant of the surfactant forming a supramolecular structure is similar to that of the surfactant in bulk (Gaines, 1966).
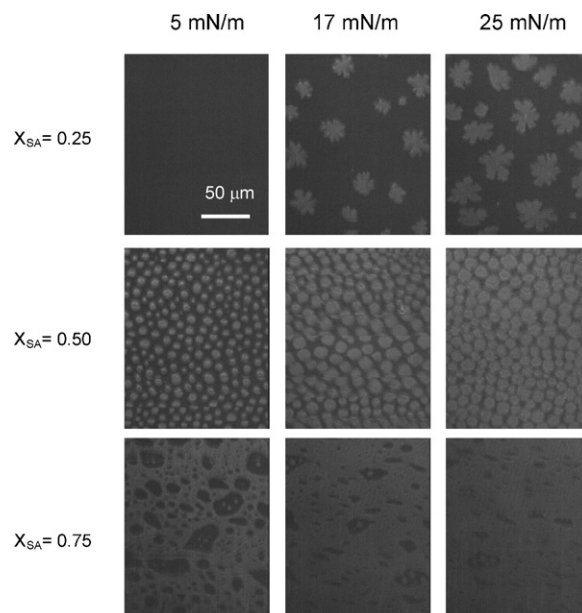
In the case of stearic acid the pKa value is 4.89. However, the surface pH (pH_s) differs from the bulk pH (pH_b) by (Gaines, 1966)

$$pH_s = pH_b + \frac{F\psi_0}{2.3RT} \quad (2)$$

In Eq. (2), ψ_0 is the double layer potential at the surface, F is the Faraday constant and RT is the thermal energy. The double layer potential depends on the ionic strength of the subphase and on the ionization degree of the surfactant.

According to the Poisson–Boltzmann equation, the surface charge density (σ) is related to the double layer potential and to the ion concentration in the bulk (C_i^∞) as:

$$\sigma = \sqrt{2RT\varepsilon_0\varepsilon} \left[\sum_i C_i^\infty \exp\left(-\frac{FZ_i\psi_0}{RT} \right) - \sum_i C_i^\infty \right]^{1/2} \quad (3)$$

The sum is taken over all the ionic species i present in the subphase, ε_0 is the permittivity in vacuum, ε the relative permittivity of the medium and Z_i is the valence of the i-ion.

On the other hand, the surface charge generated by a monolayer with an average molar area A, formed by ionizable surfactant with acid constant K_a^s, according to which the species distribution (α) depends on the surface proton concentration $[H^+]_s$, is given by:

$$\sigma = -\frac{F\alpha}{A} = -\frac{F}{A} \left(\frac{K_a^s}{K_a^s + [H^+]_s} \right) \quad (4)$$

The combination of Eqs. (1)–(3) leads to

$$0 = \sqrt{2RT\varepsilon\varepsilon_0} \left[\sum_i C_i^\infty \exp\left(\frac{-Fz_i\psi_0}{RT} \right) - \sum_i C_i^\infty \right]^{1/2}$$

$$+ \frac{F}{A} \left[\frac{K_a^s}{K_a^s + [H^+]_b \exp(-F\psi_0\alpha/RT)} \right] \quad (5)$$

This equation can be solved numerically for each bulk pH value, if all the other parameters are known.

As explained in Section 2, we performed the experiments on two different subphase compositions: 10 mM EDTA and 10 mM TRIS ("low" ionic strength), and both buffers plus 0.5 M NaCl ("high
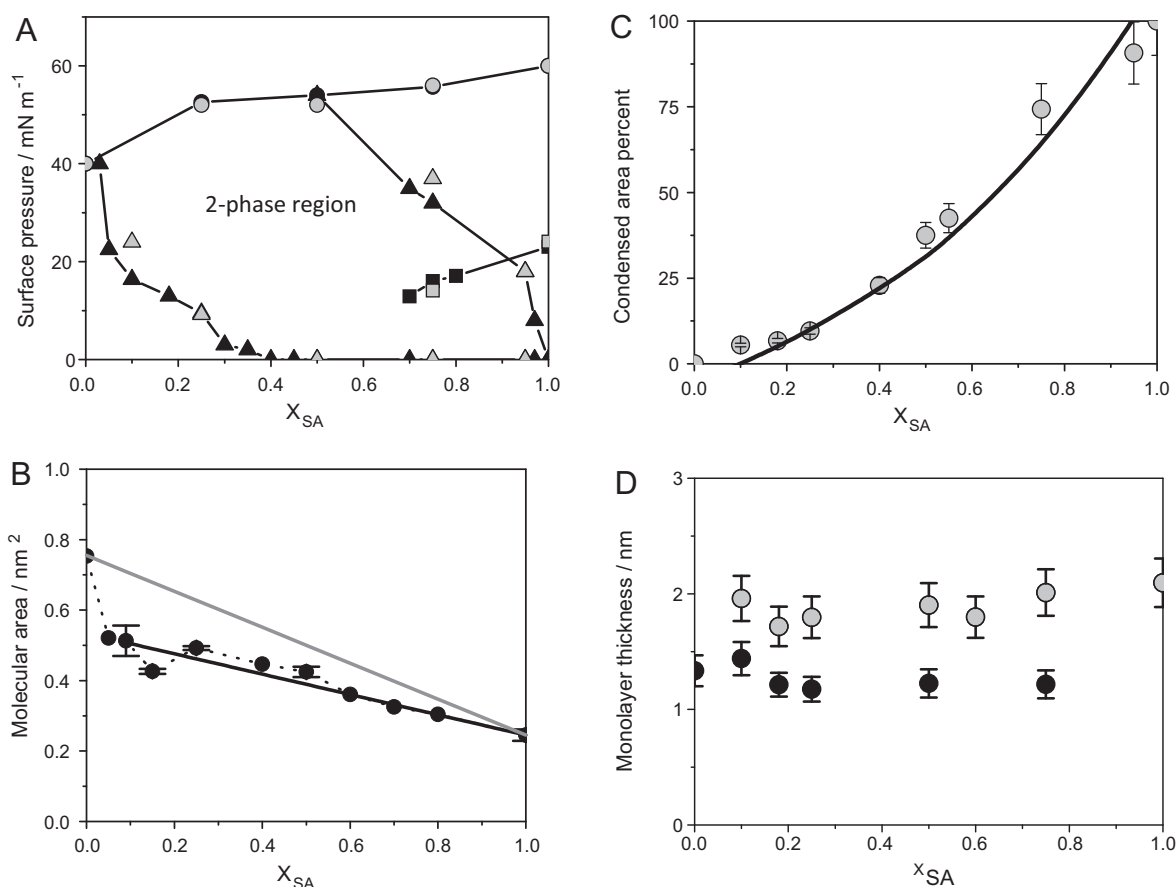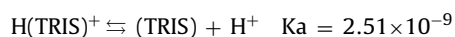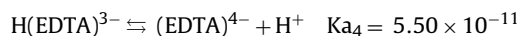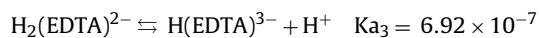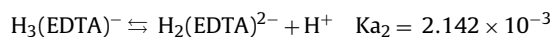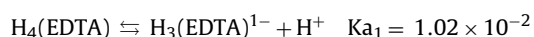
Fig. 4. Experimental parameters for mixed monolayers of dimyristoylphosphatidylcholine and stearic acid as a function of the mole fraction of stearic acid at pH 4 and 20 °C. (A) Phase diagram obtained from the compression isotherms and from monolayer images for monolayers on subphases composed of NaCl 0.5 M, EDTA 10 mM and TRIS 10 mM (black symbols) or EDTA 10 mM and TRIS 10 mM (grey symbols). Triangles: pressures where the domains first appear or disappear in the images. Squares: pressures where the kink in the isotherm is observed. Circles: collapse pressure taken from the isotherm. (B) Average molecular area taken from the isotherms at 17 mN m^{-1} (dots). The lines represent the ideal behavior (grey) and the expected result considering the lever rule and the phase diagram of figure A (black). The error bars correspond to the standard deviation of at least three independent measurements. (C) Percent of condensed area obtained from the monolayer images (dots). The line represents the expected behavior considering two phases in coexistence with composition DMPC/SA 81/9 and 5/95 (see text). The error bars correspond to the standard deviation of at least three different micrographs taken with BAM and/or FM. (D) Monolayer thickness obtained from the Brewster angle microscopy images as explained in the experimental section. Black dots: expanded phase and pure DMPC, grey dots: condensed phase and pure SA. The error bars correspond to the standard deviation of the grey level intensity of different zones of a micrograph.

ionic strength). In the latter condition, the former equations cannot be applied since they neglect ion size and ion–ion interactions. In the case of "low" ionic strength, the ion concentrations present in the system are those of the buffer ions (EDTA and TRIS). The species distribution of both molecules depends on pH according to the following equations (Skoog et al., 2005; El-Harakany et al., 1984):

$$H_4(EDTA) \leftrightharpoons H_3(EDTA)^{1-} + H^+ \quad Ka_1 = 1.02 \times 10^{-2}$$

$$H_3(EDTA)^- \leftrightharpoons H_2(EDTA)^{2-} + H^+ \quad Ka_2 = 2.142 \times 10^{-3}$$

$$H_2(EDTA)^{2-} \leftrightharpoons H(EDTA)^{3-} + H^+ \quad Ka_3 = 6.92 \times 10^{-7}$$

$$H(EDTA)^{3-} \leftrightharpoons (EDTA)^{4-} + H^+ \quad Ka_4 = 5.50 \times 10^{-11}$$

$$H(TRIS)^+ \leftrightharpoons (TRIS) + H^+ \quad Ka = 2.51 \times 10^{-9}$$

Taking all the above into account, the double layer ionic potential at the surface can be calculated for each bulk pH, and therefore the surface pH and the ionization degree of the surfactant can be known. The results for a stearic acid monolayer at 0.25 nm^2 and a subphase composed of EDTA 10 mM and TRIS 10 mM are shown in

Fig. 1. In particular, Fig. 1C shows that, depending on the degree of ionization, the interfacial pH can be as much as 4 pH units lower than the bulk pH. Fig. 1B shows that the degree of ionization is 0.5 for a bulk pH of 7.6 (in other words, the "apparent" pKa value).

This theoretical result was confirmed by the determination of the surface potential of SA monolayers on subphases at different pHs and low ionic strength. The double layer potential at each pH was subtracted from the measured surface potential, which leads to the dipole potential generated by the surfactant. This potential should increase when the molecule is ionized since a negative charge appears in the lower plane of the monolayer. Fig. 1D shows the dipole potential at 0.25 nm^2 as a function of the bulk pH. The dipole potential change generated by the ionization is in the order of the error of measurement for this parameter. However, there is an abrupt change of the potential generated by the molecules between pH 7.2 and 8.1, in agreement with the theoretical results.

According to Fig. 1B, it is possible to state that at pH 4 the surfactant is essentially neutral while at pH 10 it is nearly fully ionized. Therefore, we analyzed the behavior of the system at those two pHs.

It is already known that at pH 4 SA forms condensed monolayers, showing a second order liquid condensed/solid phase transition at about 25 mN/m at 20 °C (Spink, 1963), while at pH 10 the isotherms

show a first order phase transition from a liquid expanded to a liquid condensed monolayer at about 8 mN/m at the same temperature (Goddard et al., 1967). On the other hand, the behavior of DMPC monolayers is independent on the subphase pH (see Fig. 2).

3.2. Phase diagram of SA/DMPC monolayers at pH 4

At pH 4, DMPC and SA hardly mix; these molecules phase separate over a wide concentration range, forming two phases that can be directly observed by FM and BAM. Fig. 3 shows representative micrograph obtained by BAM at different lateral pressures and lipid proportions. The condensed domains are flower-like or rounded depending on the proportion of SA and on the compression rate.

Fig. 4A shows the phase diagram at pH 4, obtained from the isotherms and from the FM and BAM images. The kink observed for pure SA monolayers appears at lower lateral pressures and becomes more diffuse as the amount of DMPC in the mixture increases until it is no longer detectable (squares). This second order phase transition is not observed by BAM or FM, either in the pure or in the mixed monolayers. The triangles in Fig. 4 correspond to the lateral pressures where domains first appear or disappear in the images while the circles corresponds to the collapse pressure taken from the isotherms.

In order to compare the behavior of the mixture at different pHs, we analyzed the properties of the monolayers at a constant lateral pressure of $17\,mN\,m^{-1}$. This pressure was selected considering that SA and DMPC hardly mix in these conditions and thus, the domains are most probably composed of nearly pure SA molecules. At $17\,mN\,m^{-1}$ the DMPC matrix accepts 9% of SA, forming a non-ideal mixture with an average molecular area smaller than the ideal (compare grey line with symbols in Fig. 4B). At higher proportions, the system is biphasic and thus, the average molecular area changes linearly with the mole fraction. The phases in coexistence are a liquid-expanded phase with a proportion DMPC/SA 81:9 and a liquid-condensed phase composed of about 95% SA. The percent of condensed phase increases as the amount of SA in the mixture increases, as shown in Fig. 4C at $17\,mN\,m^{-1}$. The line in this figure was calculated considering that two phases coexist over the whole range corresponding to the proportions DMPC/SA 81/9 and 5/95 and with average molecular areas of 0.51 and $0.26\,nm^2$, respectively (obtained from Fig. 4B). The average height of each phase is shown in Fig. 4D; it can be observed that 9% of SA in the mixture does not modify the thickness of the expanded phase, which is similar to that found for monolayers of pure DMPC. This is expected since only 9% of the molecules correspond to SA. However, this low proportion generates a condensation of the molecular packing of about 70%, compared to the ideal monolayer (see Fig. 4B). Similarly, the condensed phase is of the same mean thickness than that of monolayers composed of pure SA. The hydrophobic mismatch between both coexisting phases is $0.6 \pm 0.2\,nm$.

The phase diagram is independent on the subphase ionic strength, as expected considering that both molecules are neutral at pH 4 and that for the two subphases used the ionic concentration is high enough to screen most electrostatic interactions.

3.3. Phase diagram of SA/DMPC monolayers at pH 10

As already mentioned, at basic pHs the monolayers of pure SA show a phase transition at about $8\,mN\,m^{-1}$ (at 20 °C); this is detected with BAM and FM by the appearance of circular domains The phase transition is also observed in the mixtures with SA, representative micrograph obtained by BAM at different lateral pressures and lipid proportions are shown in Fig. 5. Fig. 6A shows the phase diagram at pH 10, obtained from the isotherms (circles and squares) and from the FM and BAM images (triangles). For mixed SA/DMPC monolayers, the transition pressure increases as
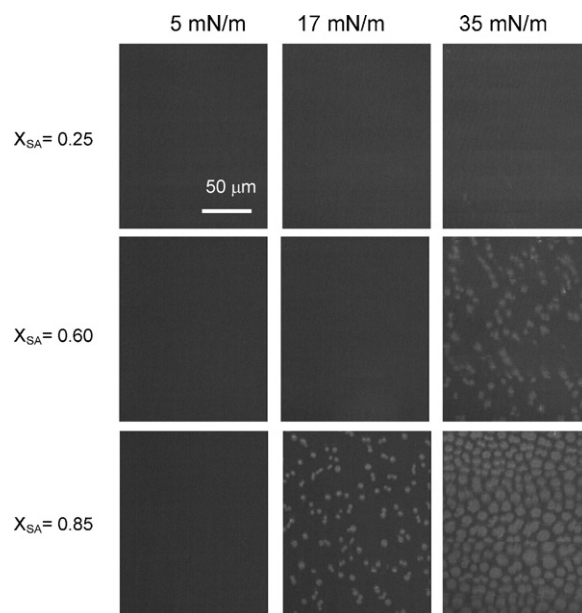
Fig. 5. Representative micrographs for monolayers of dimyristoylphosphatidylcholine and stearic acid in the indicated lipid proportions and surface pressures obtained with Brewster angle microscopy at 20 °C. Subphase composition: NaCl 0.5 M, EDTA 10 mM and TRIS 10 mM, pH 10. Images size: $150\,\mu m \times 185\,\mu m$.

the amount of DMPC increases merging with the collapse point for 25% of SA. The increase in the transition pressure indicates that DMPC mixes preferentially with the liquid-expanded phase of SA. The transition pressure coincides with the appearance of domains over all the range of DMPC proportions (Fig. 6A).

At pH 10, the behavior at low and high ionic strength is slightly different. The subphases with the lower ionic strength show the phase transition in the isotherms and the presence of domains at lower surface pressures (about $3\,mN\,m^{-1}$, see Fig. 6A). This is contrary to what should be expected according to electrostatics since high salt concentrations should screen the coulombic repulsion between the charged head groups and stabilize the condensed phase. However, the observed effect is not likely electrostatic since the ionic concentration in both solutions is high enough to screen the electrostatic effects. The decrease of the surface pressure for the phase transition may be related to a disrupting effect of the Na^+ ions on the hydrogen bonding network (Mountain and Thirumalai, 2004) that it is known to form by ionized carboxylic acids (Miranda et al., 1998).

Fig. 6B and C shows the molecular area and thickness of each phase, respectively. As already mentioned, the phase transition of pure SA monolayers occurs at higher lateral pressure the higher the amount of DMPC in the mixture. At $17\,mN\,m^{-1}$ the monolayer is in an expanded state or a condensed state depending on the amount of DMPC in the mixture. For mixtures with up to 22% of DMPC (see Fig. 6A), the monolayers are expanded, while lower amounts of DMPC lead to a condensation of the monolayer at this pressure. Since we wanted to analyze the effect of DMPC on the expanded state of the SA monolayers, in Fig. 6B we plotted the experimental molecular areas at $17\,mN\,m^{-1}$ (black symbols); and also the extrapolated molecular areas of the putative expanded monolayer at this pressure (open symbols), in other words, the expected molecular area of the monolayer in an expanded state at $17\,mN\,m^{-1}$. The grey line is the ideal behavior of the monolayer if it would be in the expanded state (considering the grey symbols at SA proportions higher than 88% and the black symbols for lower). This figure shows that the mixture in the expanded phase is not ideal but exhibits positive deviations. The thicknesses of the condensed and expanded phases are similar to those found at pH 4. The height of
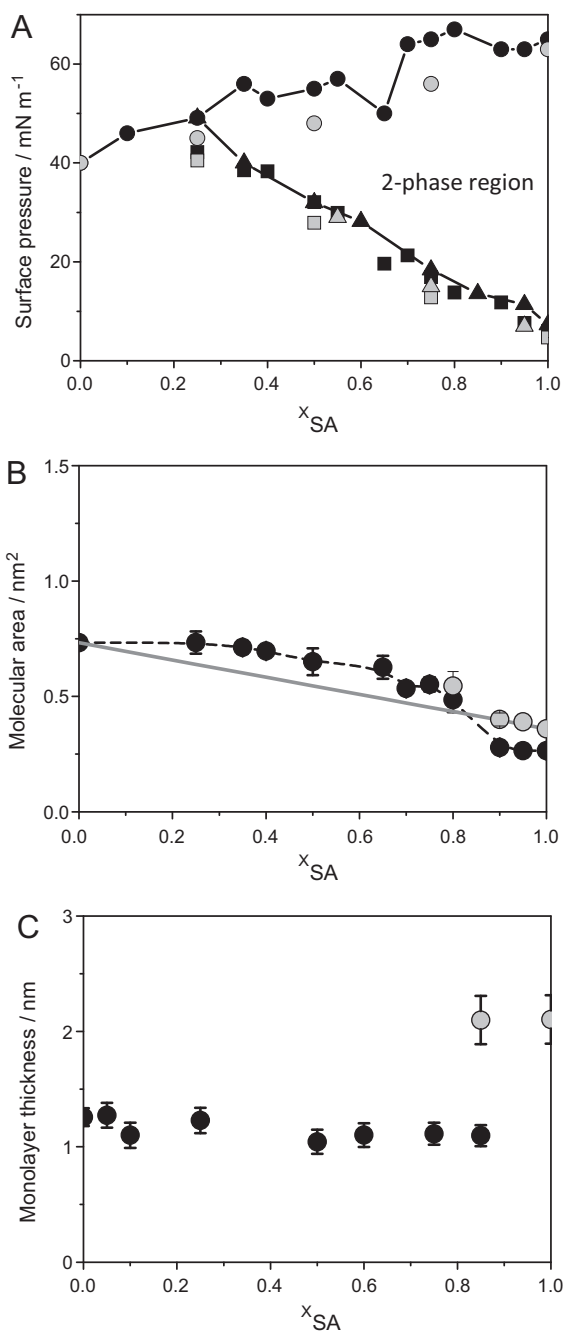
Fig. 7. Mole fraction of stearic acid at which phase segregation occurs at 17 mN m^{-1} and 20 °C on subphases at the indicated pHs. Grey lines: the phase transition is driven by pH changes at constant surface pressure. Symbols: the phase transition is driven by compression at constant pH. Subphase composition: NaCl 0.5 M, EDTA 10 mM and TRIS 10 mM (circles) or CaCl$_2$ 20 mM and TRIS 10 mM (triangles).

the condensed phase is similar to that of the pure SA monolayer, and that of the expanded phase to that of the pure DMPC film, further indicating that SA expands when mixed in the DMPC matrix.

3.4. Effect of pH at 17 mN m^{-1}

Fig. 7 shows the proportion at which the one phase-two phase structural transition occurs at 17 mN m^{-1} as a function of the sub-phase pH. As described in Section 3.2, the liquid-condensed phase of SA monolayers hardly mixes with DMPC (only to about 9% SA). However, as the pH increases the SA monolayer turns more fluid and the amount of SA admitted in the DMPC phase increases. In Fig. 7, an abrupt change around 7.6 (the apparent pKa) is observed, indicating that the miscibility of SA in the DMPC monolayer is highly related to the degree of ionization of the SA molecules.

To ensure that the phase diagrams shown in Figs. 4A and 6A correspond to, at least apparent, equilibrium states the follow-ing experiment was performed. The monolayer was compressed up to 17 mN m^{-1} on subphases at pH 4 (or 10). Then, at constant pressure the subphase pH was slowly changed while continuously observing the monolayer by fluorescence microscopy and the pH at which disappearance (or appearance) of domains occurred was reg-istered. This was carried out with monolayer proportions of 20, 30, 40 and 50% of SA. The pH ranges over which the phase transitions were observed at each proportion are plotted as grey lines in Fig. 7. Compared to the compression-driven process, appearance and dis-appearance of domains did not occur at the same points, suggesting that there may likely be a kinetically limited process; furthermore, if the system is quickly compressed (by increasing about 5-fold the compression rate), the pressure where the domains appear does not coincide with the pressure of domain disappearance. However, the surface pressure point for the phase transition caused by com-pression coincides with the range observed in the process driven by pH changes, indicating apparent equilibrium.

As already mentioned, the amount of SA admitted by the DMPC phase depends on pH (and thus on the state of ionization of SA), probably because it depends on how expanded is the SA phase. In such case, the pH dependence should not occur on subphases that contain Ca^{2+} ions because in that condition the isotherms of SA monolayers are always condensed (Goddard et al., 1967). The trian-gles in Fig. 7 shows the proportion of SA at which phase segregation is observed at 17 mN m^{-1} as a function of the subphase pH for sub-phases containing 20 mM of CaCl$_2$ (and without EDTA). These data

Fig. 6. Experimental parameters for mixed monolayers of dimyristoylphosphatidyl-choline and stearic acid as a function of the mole fraction of stearic acid at pH 10 and 20 °C. (A) Phase diagram obtained from the compression isotherms and from mono-layer images for monolayers on subphases composed of NaCl 0.5 M, EDTA 10 mM and TRIS 10 mM (black symbols) or EDTA 10 mM and TRIS 10 mM (grey symbols). Tri-angles: pressures where the domains first appear in the images. Squares: pressures where the phase transition in the isotherm is observed. Circles: collapse pressure taken from the isotherm. (B) Average molecular area taken from the isotherms at 17 mN m^{-1} (black dots) and extrapolated assuming that the monolayer remains expanded at this pressure and proportions (grey dots). The line represents the ideal behavior. The error bars correspond to the standard deviation of at least three inde-pendent measurements. (C) Monolayer thickness obtained from the Brewster angle microscopy images as explained in the experimental section. Black dots: expanded phase and pure DMPC, grey dots: condensed phase and pure stearic acid. The error bars correspond to the standard deviation of the grey level intensity of different zones of a micrograph.
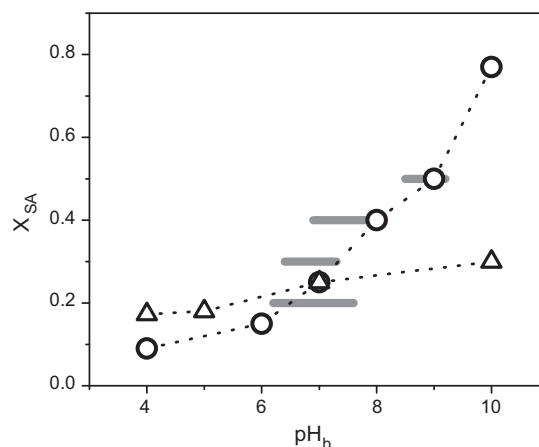
clearly show that the pH dependence is less marked when Ca^{2+} is present in the subphase, confirming that the condensation state of SA is an important factor for its mixing with DMPC.

4. Conclusions

In this work we analyzed the effect of charge on the phase diagram of binary monolayers, and thus on the intermolecular interaction. We showed that a neutral molecule that forms expanded monolayer mixes well with a charged molecule but not with the same molecule in the neutral state, and that this is related to its degree of ionization. For the systems studied the ionizable molecule acquires more disorder when the molecule is charged and forms very condensed monolayers when the molecule is neutral or when Ca^{2+} ions are present in the subphase. All these results indicate that the mixing of SA with DMPC is highly related to the disorder in the hydrocarbon chain, which in turn depends on the presence of charges in the polar head group of the SA molecules. The electrostatic interactions are not the determining factor for the phase segregation but they contribute indirectly, through the regulation of the disorder of the hydrocarbon chain.

The phase diagrams were constructed with transition points induced by monolayer compression. On the other hand, at an average packing density the lateral pressure exhibits fluctuations depending on the membrane elasticity (Phillips et al., 1975; Sackmann, 1995) and it is not a constant control parameter at the local level. In a cell membrane however the local surface pH can vary over values spanning the range of pHs studied in this work. In that sense, Fig. 7 shows that the results found do not depend on the manner in which the process is driven, and thus the same effects can be induced by local pH changes or by surface pressure. Thus, this could be a way of recruiting or expelling ionizable molecules into and from a defined mixed lipid phase thus controlling lateral domain segregation which, in turn, can be further controlled by the presence of bivalent ions.

Acknowledgements

References

Adamson, A.W., 1982. Physical Chemistry of Surfaces. Wiley, New York.

Almeida, P.F.F., 2009. Thermodynamics of lipid interactions in complex bilayers. Biochim. Biophys. Acta Biomembr. 1788, 72–85.

Brezesinski, G., Möhwald, H., 2002. Langmuir monolayers to study interactions at model membrane surfaces. Adv. Colloid Interf. Sci. 100–102, 563–584.

Bringezu, F., Ding, J., Brezesinski, G., Zasadzinski, J.A., 2001. Changes in model lung surfactant monolayers induced by palmitic acid. Langmuir 17, 4641–4648.

Brockman, H., 1999. Lipid monolayers: why use half a membrane to characterize protein–membrane interactions? Curr. Opin. Struct. Biol. 9, 438–443.

Deamer, D.W., Meek, D.W., Cornwell, D.G., 1967. Properties, composition, and structure of stearic acid-stearate monolayers on alkaline earth solutions. J. Lipid Res. 8, 255–263.

Ducharme, D., Max, J.J., Salesse, C., Leblanc, R.M., 1999. Ellipsometric study of the physical states of phosphatidylcholines at the air–water interface. J. Phys. Chem. 94, 1925–1932.

El-Harakany, A.A., Abdel Halima, F.M., Barakat, A.O., 1984. Dissociation constants and related thermodynamic quantities of the protonated acid form of tris-(hydroxymethyl)-aminomethane in mixtures of 2-methoxyethanol and water at different temperatures. J. Electroanal. Chem. 162, 285–305.

Fanani, M.L., Hartel, S., Oliveira, R.G., Maggio, B., 2002. Bidirectional control of sphingomyelinase activity and surface topography in lipid monolayers. Biophys. J. 83, 3416–3424.

Fanani, M.L., Hartel, S., Maggio, B., De Tullio, L., Jara, J., Olmos, F., Oliveira, R.G., 2010. The action of sphingomyelinase in lipid monolayers as revealed by microscopic image analysis. Biochim. Biophys. Acta 1798, 1309–1323.

Gaines Jr., G.L., 1966. Insoluble Monolayers at Liquid–Gas Interfaces. Wiley, New York.

Goddard, E.D., Kao, O., Kung, C., 1967. Monolayer properties of fatty acids IV. Influence of cation at high pH. J. Colloid Sci. 24, 297–309.

Hermelink, A., Brezesinski, G., 2008. Do unsaturated phosphoinositides mix with ordered phosphadidylcholine model membranes? J. Lipid Res. 49, 1918–1925.

Koynova, R., Tenchov, B., 2001. Interactions of surfactants and fatty acids with lipids. Curr. Opin. Colloid Interf. Sci. 6, 277–286.

Langner, M., Kubica, K., 1999. The electrostatics of lipid surfaces. Chem. Phys. Lipids 101, 3–35.

Lhevender, C., Meunier, J., Hénon, S., 2000. Brewster angle microscopy. In: Baszkin, A., Dahlen, W. (Eds.), Physical Chemistry of Biological Interfaces. Marcel Dekker, Inc., New York, pp. 559–576.

Maggio, B., Lucy, J.A., 1975. Studies on mixed monolayers of phospholipids and fusogenic lipids. Biochem. J. 149, 597–608.

Maggio, B., Lucy, J.A., 1976. Polar-group behaviour in mixed monolayers of phospholipids and fusogenic lipids. Biochem. J. 155, 353–364.

Maggio, B., 1994. The surface behavior of glycosphingolipids in biomembranes: a new frontier of molecular ecology. Prog. Biophys. Mol. Biol. 62, 55–117.

Maggio, B., Fanani, M.L., Rosetti, C.M., Wilke, N., 2006. Biophysics of sphingolipids II. Glycosphingolipids: an assortment of multiple structural information transducers at the membrane surface. Biochim. Biophys. Acta 1758, 1922–1944.

Maggio, B., Borioli, G.A., Del Boca, M., De Tullio, L., Fanani, M.L., Oliveira, R.G., Rosetti, C.M., Wilke, N., 2008. Composition-driven surface domain structuring mediated by sphingolipids and membrane-active proteins, above the nano- but under the micro-scale: mesoscopic biochemical/structural cross-alk in biomembranes. Cell Biochem. Biophys. 50, 79–109.

McConnell, H.M., 1991. Structures and transitions in lipid monolayers at the air–water interface. Annu. Rev. Phys. Chem. 42, 171–195.

Mengistu, D.H., Bohinc, K., May, S., 2010. A model for the electrostatic contribution to the pH-dependent nonideal mixing of a binary charged–zwitterionic lipid bilayers. Biophys. Chem. 150, 112–118.

Miranda, P.B., Du, Q., Shen, Y.R., 1998. Interaction of water with a fatty acid Langmuir film. Chem. Phys. Lett. 286, 1–8.

Möhwald, H., 1990. Phospholipid and phospholipid–protein monolayers at the air/water interface. Annu. Rev. Phys. Chem. 41, 441–476.

Möhwald, H., Dietrich, A., Böhm, C., Brezesinski, G., Thoma, M., 1995. Domain formation in monolayers. Mol. Membr. Biol. 12, 29–38.

Mountain, R.D., Thirumalai, D., 2004. Alteration in water structure induced by guanidinium and sodium ions. J. Phys. Chem. B 18, 19711–19716.

Petrov, J.G., Pfohl, T., Möhwald, H., 1999. Ellipsometric chain length dependence of fatty acid Langmuir monolayers. A heads-and-tails model. J. Phys. Chem. B 103, 3417–3424.

Phillips, M.C., Graham, D.E., Hauser, H., 1975. Lateral compressibility and penetration into phospholipid monolayers and bilayer membranes. Nature 254, 154–156.

Roach, C., Feller, S.E., Ward, J.A., Saame, Shaikh, R., Zerouga, M., Stillwell, W., 2004. Comparison of Cis and Trans fatty acid containing phosphatidylcholines on membrane properties. Biochemistry 43, 6344–6351.

Romão, R.I.S., Gonçalves da Silva, A.M., 2004. Phase behaviour and morphology of binary mixtures of DPPC with stearonitrile, stearic acid, and octadecanol at the air–water interface. Chem. Phys. Lipids 131, 27–39.

Sackmann, E., 1995. Physical basis of self-organization and function of membranes: physics of vesicles. In: Lipowsky, R., Sackmann, E. (Eds.), Structure and Dynamics of Membranes. From Cells to Vesicles. Elsevier, Amsterdam, pp. 213–304.

Schmidt, R., Meier, U., Yabut-Perez, M., Walmrath, D., Grimminger, F., Seeger, W., Günther, A., 2001. Alteration of fatty acid profiles in different pulmonary surfactant phospholipids in acute respiratory distress syndrome and severe pneumonia. Am. J. Respir. Crit. Care Med. 163, 95–100.

Schullery, S.E., Seder, T.A., Weinstein, D.A., Bryant, D.A., 1981. Differential thermal analysis of dipalmitoylphosphatidylcholine-fatty acid mixtures. Biochemistry 20, 6818–6824.

Skoog, A., Douglas, West, D.M., Holler, F.J., Crouch, S.R., 2005. Fundamentos de Química Analítica. Thomson Learning, p. 468, Ch 17.

Spink, J.A., 2005. Ionization of monolayers of fatty acids from C14 to C18. J. Colloid Sci. 18, 512–525.

Templer, R.H., Seddon, J.M., Warrender, N.A., Syrykh, A., Huang, Z., Winter, R., Erbes, J., 1998. Inverse bicontinuous cubic phases in 2:1 fatty acid/phosphatidylcholine mixtures. The effects of chain length, hydration, and temperature. J. Phys. Chem. B 102, 7251–7261.

Villasuso, A.L., Wilke, N., Maggio, B., Machado, E., 2010. The surface organization of diacylglycerol pyrophosphate and its interaction with phosphatidic acid at the air–water interface. Chem. Phys. Lipids 163, 771–777.

Vollhardt, D., 2002. Supramolecular organisation in monolayers at the air/water interface. Mater. Sci. Eng. C 22, 121–127.

Wilke, N., Maggio, B., 2009. J. Phys. Chem. B 113, 12844–12851.